Cooperazione Culturale. The work was also supported by the project No. TR-11033 of the Serbian Ministry of Science and Technological Development.

REFERENCES

1. G. Dambrine, A. Cappy, F. Heliodore, and E. Playez, A new method for determining the FET small signal equivalent circuit, IEEE Trans Microwave Theory Tech 36 (1988), 1151-1159.
2. M. Berroth and R. Bosch, Broad-band determination of the FET small signal equivalent circuit, IEEE Trans Microwave Theory Tech 38 (1990), 891-895.
3. N. Rorsman, M. Garcia, C. Karlsson, and H. Zirath, Accurate small signal modeling of HFETs for millimeter-wave applications, IEEE Trans Microwave Theory Tech 44 (1996), 432-437.
4. A. Caddemi, G. Crupi, and A. Macchiarella, On-wafer scaled GaAs HEMTs: Direct and robust small signal modeling up to 50 GHz, Microwave Opt Technol Lett 51 (2009), 1958-1963.
5. G. Crupi, D.M.M.-P. Schreurs, A. Raffo, A. Caddemi, and G. Vannini, A new millimeter wave small signal modeling approach for pHEMTs accounting for the output conductance time delay, IEEE Trans Microwave Theory Tech 56 (2008), 741-746.
6. G. Crupi, D.M.M.-P. Schreurs, and A. Caddemi, On the small signal modeling of advanced microwave FETs: A comparative study, Int J RF and Microwave Comput-Aided Eng 18 (2008), 417-425.
7. P.M. Watson, M. Weatherspoon, L. Dunleavy, and G.L. Creech, Accurate and efficient small-signal modeling of active devices using artificial neural networks, In: Proceedings of Gallium Arsenide Integrated Circuit Symposium, Technical Digest, Baltimore, MD, 1998, pp. 95–98.
8. V. Marković, O. Pronić, and Z. Marinković, Noise wave modeling of microwave transistors based on neural networks, Microwave Opt Technol Lett 41 (2004), 294-297.
9. Z. Marinković and V. Marković, Temperature dependent models of low-noise microwave transistors based on neural networks, Int J RF Microwave CE 15 (2005), 567-577.
10. Z. Marinković, O. Pronić, and V. Marković, Bias-dependent scalable modeling of microwave FETs based on artificial neural networks, Microwave Opt Technol Lett 48 (2006), 1932-1936.
11. Q.J. Zhang and K.C. Gupta, Neural networks for RF and microwave design, Artech House, Norwood, MA, 2000.
12. H. Taher, D. Schreurs, and B. Nauwelaers, Constitutive relations for nonlinear modeling of Si/SiGe HBTs using an ANN model, Int J RF Microwave CE 15 (2005), 203-209.

SMALL-SIZE INTERNAL EIGHT-BAND LTE/WWAN MOBILE PHONE ANTENNA WITH INTERNAL DISTRIBUTED LC MATCHING CIRCUIT

Kin-Lu Wong,[1] Wei-Yu Chen,[1] Chun-Yih Wu,[2] and Wei-Yu Li[2]
[1] Department of Electrical Engineering, National Sun Yat-Sen University, Kaohsiung 80424, Taiwan; Corresponding author: wongkl@ema.ee.nsysu.edu.tw
[2] Information and Communications Research Laboratories, Industrial Technology Research Institute, Hsinchu 31040, Taiwan

Received 25 December 2009

ABSTRACT: *A coupled-fed planar inverted-F antenna (PIFA) to be mounted at the small no-ground portion of the system circuit board of the mobile phone with a low profile of 10 mm to the system ground plane and a thin profile of 3 mm to the system circuit board is presented. The proposed small-size PIFA is formed by a simple structure of two radiating strips of different lengths, both capacitively fed by a coupling feed and short circuited to the system ground plane by a shorting strip. The coupling feed and shorting strip together function as an internal distributed LC matching circuit, with the coupling feed as a capacitive element and the shorting strip as an inductive element. This internal distributed LC matching circuit has an equivalent layout as the conventional external high-pass LC matching circuit with lumped elements; both are effective in tuning the antenna's lower band bandwidth. In addition, the antenna with the proposed internal distributed LC matching circuit, in this study, can lead to much widened bandwidths in both the antenna's lower and upper bands to cover the 698–960 and 1710–2690 MHz bands, respectively. That is, eight-band LTE/WWAN operation can be achieved. Results of the proposed antenna with the internal distributed LC matching circuit are presented.* © 2010 Wiley Periodicals, Inc. Microwave Opt Technol Lett 52:2244–2250, 2010; Published online in Wiley InterScience (www.interscience.wiley.com). DOI 10.1002/mop.25431

Key words: *mobile antennas; handset antennas; internal mobile phone antennas; LTE/WWAN antennas*

1. INTRODUCTION

Recently, it has been demonstrated that by using a coupling feed, the type of planar inverted-F antenna (PIFA) with no back ground plane for WWAN operation can have dual-resonance excitation in the antenna's lower band at about 900 MHz [1–6] or excite its 1/8-wavelength resonant mode as the antenna's lowest resonant mode [7–9]. The former leads to a wide lower band to cover the GSM850/900 operation (824–960 MHz) for the PIFA without increasing its occupied volume, while the latter results in a compact size for the PIFA to operate at about 900 MHz. In the reported studies of such coupled-fed PIFAs [1–9], the design considerations mainly focus on the coupling feed only; tuning the shorting strip to incorporate with the coupling feed to achieve much widened bandwidths of the PIFA is not included in the study.

In this article, we propose that the coupling feed and the shorting strip together can be considered as an internal distributed LC matching circuit for the coupled-fed PIFAs. That is, the coupling feed can be treated as a capacitive element, while the shorting strip is considered as an inductive element [10, 11]. More specifically, this internal distributed LC matching circuit has an equivalent layout as the conventional external high-pass LC matching circuit with lumped elements [12–15] (see Fig. 2), which is effective in tuning the antenna's lower band bandwidth. In the internal distributed matching circuit, the equivalent capacitance and inductance in the matching circuit can be adjusted by tuning the dimensions of the coupling feed and the shorting strip. The obtained bandwidths of the proposed PIFA can then be effectively widened.

By applying the design concept of the proposed internal distributed LC matching circuit to the PIFA with a simple structure of two radiating strips of different lengths, large bandwidths in both the antenna's lower and upper bands are easily achieved. The operating bands of 698–960 MHz (LTE700/GSM850/900) and 1710–2690 MHz (GSM1800/1900/UMTS/LTE2300/2500) have been obtained for the proposed PIFA with a thin profile of 3 mm and a low profile of 10 mm to be mounted at the small no-ground portion of the system circuit board of the mobile phone. Notice that the LTE operation [16, 17] in the 700 MHz (698–787 MHz), 2300 MHz (2305–2400 MHz), and 2500 MHz bands (2500–2690 MHz) is recently introduced, which can provide better mobile broadband and multimedia services than the existing WWAN operation including the GSM (GSM850/900, 824–960 MHz and GSM1800/1900, 1710–1990 MHz) and UMTS (1920–2170 MHz) [18]. This makes the eight-band LTE/WWAN operation in the 698–960 and 1710–2690 MHz bands

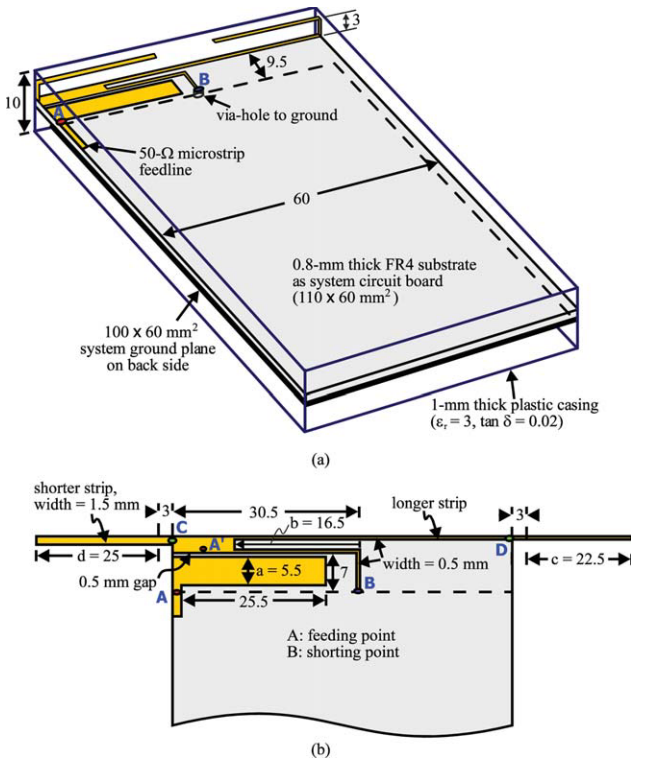

Figure 1 (a) Geometry of the proposed PIFA with an internal distributed LC matching circuit for eight-band LTE/WWAN operation in the mobile phone. (b) Dimensions of the antenna's metal pattern. [Color figure can be viewed in the online issue, which is available at www.interscience.wiley.com]

very attractive for mobile phone users. Details of the obtained results, including the SAR values [19] with the presence of the head and hand phantoms [20], are presented and discussed.

2. PROPOSED ANTENNA

Figure 1(a) shows the geometry of the proposed small-size PIFA with an internal distributed LC matching circuit for eight-band LTE/WWAN operation in the mobile phone. The detailed dimensions of the metal pattern of the PIFA are given in Figure 1(b). A 1-mm thick plastic casing of relative permittivity 3.0 and loss tangent 0.02 is used as the mobile phone casing in the study. In the proposed PIFA, there are two radiating strips (the longer and shorter radiating strips) connected at point A' to the internal LC matching circuit formed by the coupling feed and the shorting strip. The coupling feed is obtained by using a long, wide feeding strip of width 5.5 mm (a) to capacitively excite the two radiating strips through a narrow gap of 0.5 mm. By varying the width a, the equivalent capacitance contributed by the coupling feed can be adjusted. That is, the coupling feed can be considered as a distributed capacitive element as shown in Figure 2. The shorting strip has a narrow width of 0.5 mm and a long length of 24 mm. By adjusting the length b in the shorting strip, the equivalent inductance contributed by the shorting strip, as shown in Figure 2, can be tuned. The parameters a and b are two major factors in effectively tuning the suitable dimensions of the internal distributed LC matching circuit for obtaining much widened bandwidths of the proposed antenna. Detailed effects of the parameters a and b are studied in Figure 6 in the next section.

Notice that the proposed internal distributed LC matching circuit has an equivalent layout as the conventional external high-pass LC matching circuit with lumped elements [12–15]. This explains that the proposed internal distributed LC matching circuit can lead to good impedance matching for frequencies over the antenna's lower band. Moreover, it is also found that the impedance matching for frequencies over the antenna's upper band can be improved to result in a widened upper band bandwidth; this is an advantage over the use of the external high-pass lumped LC matching circuit.

The front end of the coupling feed at point A is the feeding point of the antenna, which is connected to a 50-Ω microstrip feedline printed on the front side of the system circuit board of the mobile phone for testing the antenna in the experiment. Notice that the internal distributed LC matching circuit formed by the coupling feed and the shorting strip is printed on the no-ground portion of the system circuit board, which is an FR4 substrate of 110 × 60 mm^2 used in the study. The no-ground portion has a small length of 10 mm above the top edge of the system ground plane (size 100 × 60 mm^2) printed on the back side of the system circuit board.

A fraction of the longer strip is also printed on the no-ground portion and is connected to point A'. The end section of the longer strip is made from a copper strip of width 0.5 mm and connected to the printed portion of the longer strip at point D on the system circuit board. With the aid of the internal distributed LC matching circuit, the longer strip can generate a wideband lower band at about 900 MHz to cover the LTE700/GSM850/900 (698–960 MHz) operation and an upper band at about 2000 MHz to cover the GSM1800/1900/UMTS (1710–2170 MHz) operation. By adding the shorter strip, which is made of a copper strip of width 1.5 mm and length 28 mm, a resonant mode at about 2600 MHz can be generated. This resonant mode incorporating the one at about 2000 MHz contributed by the longer strip leads to a very wide upper band to cover the GSM1800/1900/UMTS/LTE2300/2500 (1710–2690 MHz) operation. In this case, eight-band LTE/WWAN operation is achieved. By tuning the lengths c and d, in the longer and shorter strips, respectively, the excited resonant modes for the desired lower and upper bands can be adjusted. Detailed effects of the lengths c and d are analyzed in Figure 7 in the next section. Also, note that both the longer and shorter strips are bent such that their open ends are extended to each other with a small height of 3 mm above the system circuit board. The small height makes the proposed

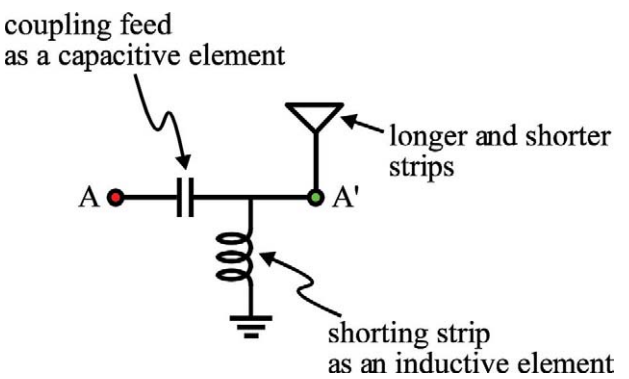

Figure 2 Internal distributed LC matching circuit formed by the coupling feed as a capacitive element and the shorting strip as an inductive element in the proposed antenna; this internal distributed matching circuit has an equivalent layout as the conventional external high-pass LC matching circuit with lumped elements. [Color figure can be viewed in the online issue, which is available at www.interscience.wiley.com]

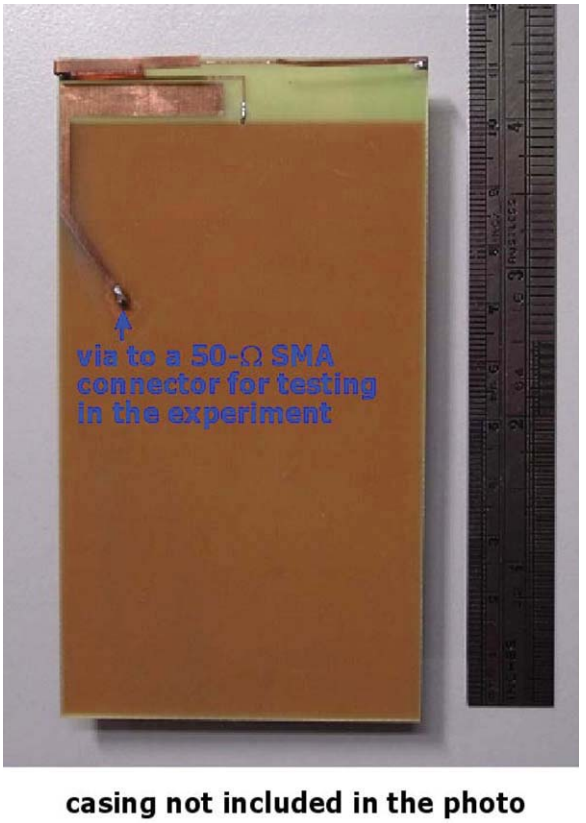

Figure 3 Photo of the fabricated antenna (casing not included in the photo). [Color figure can be viewed in the online issue, which is available at www.interscience.wiley.com]

antenna with a thin profile, which is especially suitable for slim mobile phone applications [21–26].

3. RESULTS AND DISCUSSION

The proposed antenna was fabricated and tested. Figure 3 shows the photo of the fabricated antenna, and results of the measured and simulated return loss are presented in Figure 4. The simulated results obtained using the Ansoft HFSS simulation software version 12 [27] are similar to the measured data. From the measurement, two wide operating bands are generated. With the definition of 3:1 VSWR (6-dB return loss), which is widely used for the internal mobile phone antenna design specification, the antenna's lower band has a wide bandwidth of 350 MHz (695–1045 MHz) and covers the LTE700/GSM850/900 operation. The antenna's upper band shows an even wider bandwidth of 1260 MHz (1640–2900 MHz) and covers the GSM1800/1900/UMTS/LTE2300/2500 operation. Hence, with the proposed antenna, the eight-band LTE/WWAN operation can be obtained.

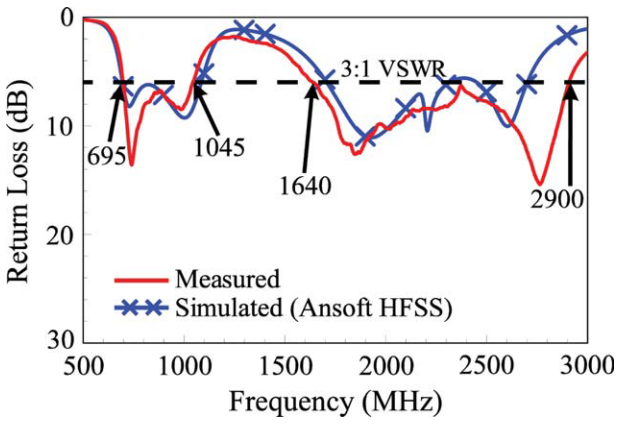

Figure 4 Measured and simulated return loss of the proposed antenna. [Color figure can be viewed in the online issue, which is available at www.interscience.wiley.com]

To analyze the operating principle of the antenna, Figure 5 shows the simulated return loss and input impedance of the proposed antenna, the case without the shorter strip (Ref1) and the case using a direct feed (Ref2). Corresponding dimensions of the three antennas studied in the figure are the same as given in Figure 1. Notice that when the internal distributed LC matching circuit is replaced by a simple direct feed, the obtained bandwidths of both the antenna's lower and upper bands are greatly decreased [see the results in Fig. 5(a)]. This is achieved by the greatly decreased input impedance matching level (both the real and imaginary parts) as seen in Figure 5(b) (see the results for Proposed and Ref1 versus Ref2). Also, the wide lower band at about 900 MHz for Proposed and Ref1 is mainly contributed by

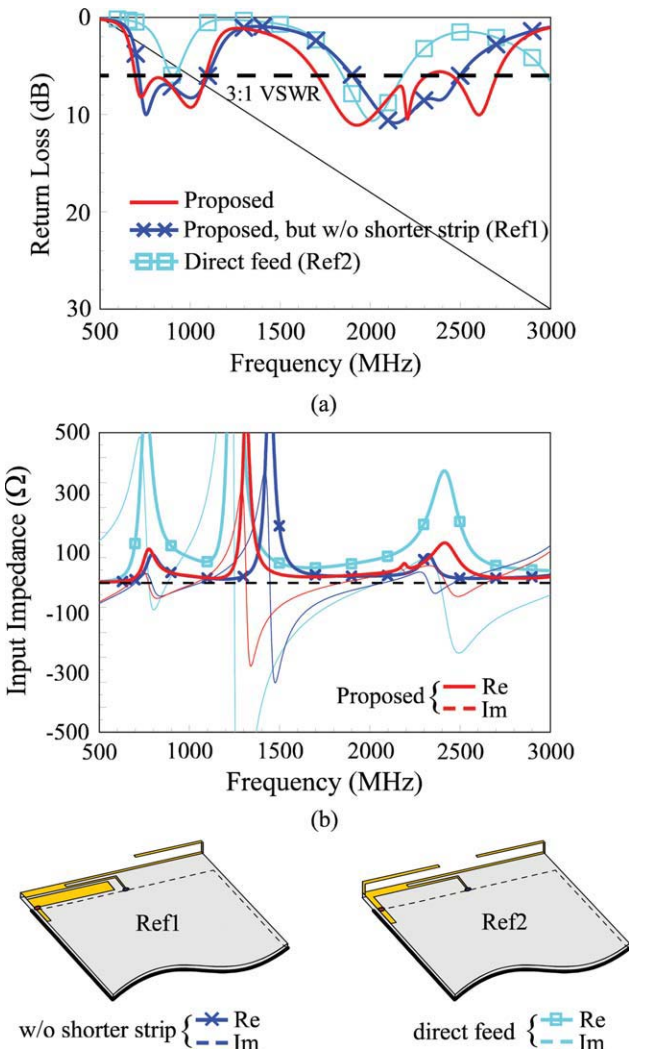

Figure 5 Simulated (a) return loss and (b) input impedance of the proposed antenna, the case without the shorter strip (Ref1), and the case using a direct feed (Ref2). Corresponding dimensions of the three antennas studied in the figure are the same as given in Figure 1. [Color figure can be viewed in the online issue, which is available at www.interscience.wiley.com]

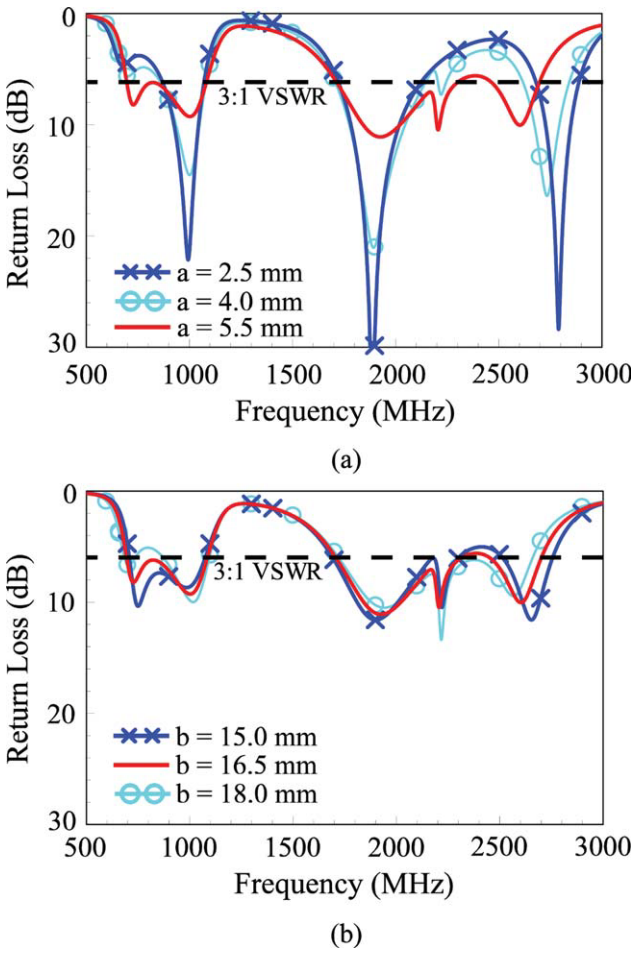

Figure 6 Simulated return loss for the proposed antenna as a function of (a) the width *a* of the feeding strip in the coupling feed and (b) the length *b* in the shorting strip. Other dimensions are the same as given in Figure 1. [Color figure can be viewed in the online issue, which is available at www.interscience.wiley.com]

the longer strip, which generates a dual-resonant fundamental mode covering the desired 698–960 MHz band. The longer strip also generates a dual-resonant higher order resonant mode at about 2200 MHz (see Ref1). By adding the shorter strip, an additional resonant mode at about 2600 MHz is generated (see the proposed), which incorporates the higher-order resonant mode contributed by the longer strip to result in a very wide operating band to cover the desired 1710–2690 MHz band.

Figure 6 shows the simulated return loss for the proposed antenna as a function of the width *a* of the feeding strip in the coupling feed and the length *b* in the shorting strip. The results for the width *a* varied from 2.5 to 5.5 mm are presented in Figure 6(a). Large effects on both the antenna's lower and upper bands are observed. Results show that a wide feeding strip is required in the coupling feed to achieve enhanced bandwidths for the antenna. In Figure 6(b), results for the length *b* varied from 15.0 to 18.0 mm are presented. Some effects on the antenna's lower and upper bands are seen, especially on the lower band. Hence, in addition to the width *a* of the feeding strip, proper selection of the length *b* of the shorting strip is also an important parameter in achieving enhanced bandwidths of the antenna.

Effects of the longer and shorter strips are analyzed in Figure 7. Results of the simulated return loss for the length *c* in the longer strip varied from 17.5 to 22.5 mm and the length *d* in the shorter strip varied from 23 to 27 mm are shown in Figures 7(a) and 7(b), respectively. For both cases of the lengths *c* and *d*, small effects are seen for the antenna's lower band. This also suggests that the lower band is mainly controlled by the internal distributed LC matching circuit as studied in Figure 6. On the other hand, the variations in the lengths *c* and *d* cause large effects on the antenna's upper band. As seen in Figure 7(b), the resonant mode at about 2600 MHz can be controlled by the length *d* in the shorter strip. The length *d* also causes some variations in the impedance matching of other frequencies in the upper band. This is largely owing to the coupling interaction between the two end sections of the longer and shorter strips facing to each other. Effects of the length *c* in the longer strip studied in Figure 7(a) are similar to those observed in Figure 7(b). That is, variations in the length *c* can also cause different coupling interaction between the two end sections of the longer and shorter strips, thus causing impedance matching variations in the resonant modes contributed by either the longer strip or the shorter strip. The obtained results indicate that to achieve good impedance matching for all frequencies over the antenna's upper band, both the lengths *c* and *d* should be adjusted in the proposed antenna.

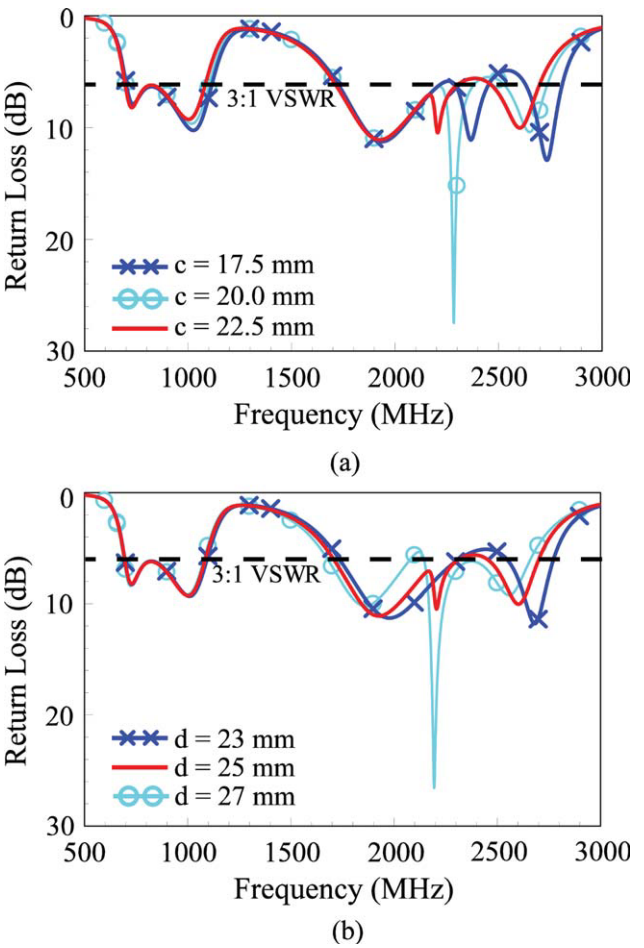

Figure 7 Simulated return loss for the proposed antenna as a function of (a) the length *c* in the longer strip and (b) the length *d* in the shorter strip. Other dimensions are the same as given in Figure 1. [Color figure can be viewed in the online issue, which is available at www.interscience.wiley.com]

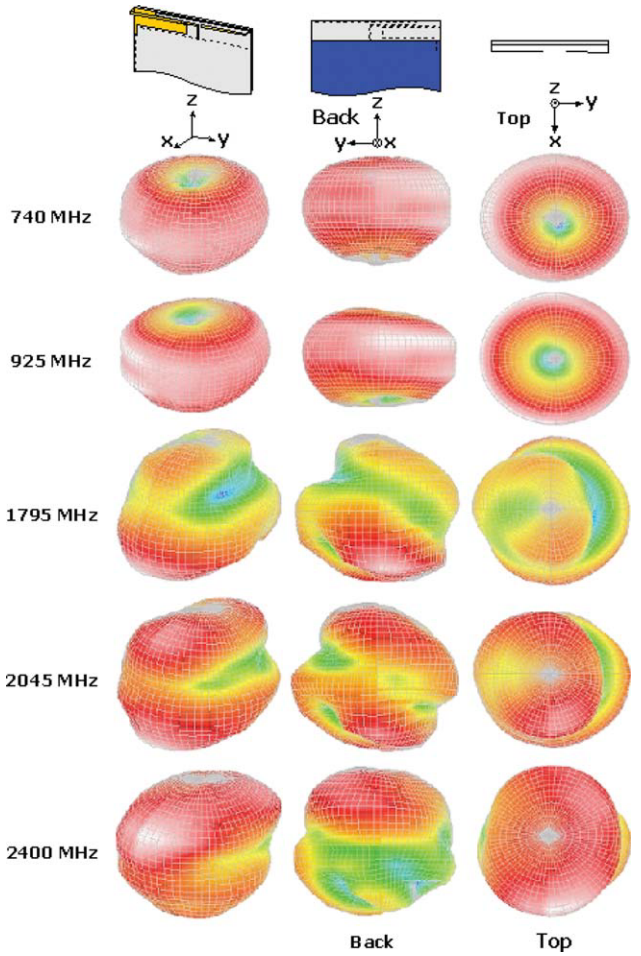

Figure 8 Measured three-dimensional (3-D) radiation patterns for the proposed antenna. [Color figure can be viewed in the online issue, which is available at www.interscience.wiley.com]

Figure 8 shows the measured three-dimensional radiation patterns for the fabricated antenna shown in Figure 2. The radiation patterns at 740, 925, 1795, 2045, and 2400 MHz are presented. Notice that at each frequency, the radiation patterns seen in three different directions are shown. For the lower frequencies at 740 and 925 MHz, near-omnidirectional radiation patterns are obtained. For the higher frequencies at 1795, 2045, and 2400 MHz, some dips or nulls are seen in the radiation pattern. The differences in the measured radiation patterns for the lower and higher frequencies are related to the excited surface currents in the system ground plane. For the lower frequencies, there are generally no current nulls excited in the system ground plane; while for the higher frequencies, current nulls are usually excited in the system ground plane owing to their shorter wavelength comparable to the length of the system ground plane. This leads to the dips or nulls seen in the radiation patterns at higher frequencies.

Figure 9 shows the measured antenna gain and radiation efficiency of the fabricated antenna. Results are measured in a far-field anchoic chamber; the lower band and upper band results are shown in Figures 9(a) and 9(b), respectively. The radiation efficiency is all better than 50% (about 52–75% for the lower band and about 53–78% for the upper band), which is acceptable for practical mobile phone applications. For the antenna gain, it is about −0.8–0.7 dBi for the lower band and about 0.8–3.2 dBi for the upper band.

To test the SAR behavior of the proposed antenna in the mobile phone, the SAR simulation model including the user's head and hand provided by SEMCAD [28] is used. The antenna including the mobile phone casing is held by the hand phantom and attached to the head phantom at the ear position. The grip of the hand phantom is shown in the figure. The distance between the palm center and the casing is 30 mm and that between the palm bottom and the casing is 15 mm; these distances are reasonable as studied in Ref. 20. Notice that the antenna is placed at the bottom of the mobile phone which has been shown to be a promising arrangement for practical applications of such antennas with no back ground plane to achieve decreased SAR values [8, 11, 20, 29]. The simulated SAR values for 1-g head tissue and 1-g head and hand tissue are listed in the table in Figure 10. The return loss given in the table shows the impedance matching level at the testing frequency. The SAR values are tested using input power of 24 dBm for the GSM850/900 operation (859 and 925 MHz) and 21 dBm for the GSM1800/1900 operation (1795 and 1920 MHz), UMTS operation (2045 MHz), and LTE operation (740, 2350, and 2595 MHz). The SAR values at lower frequencies are about the same for the cases with and without the hand phantom. Conversely, large effects of the hand phantom on the obtained SAR values are seen at higher frequencies, especially at 2595 MHz. This is related to the smaller wavelengths at higher frequencies, which are comparable to the dimensions of the fingers of the hand

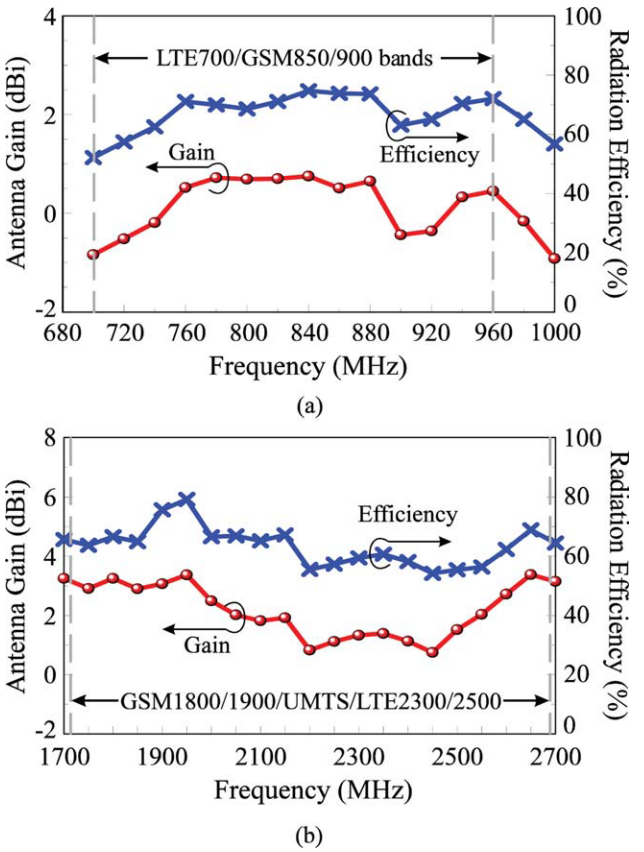

Figure 9 Measured antenna gain and radiation efficiency of the proposed antenna. (a) The lower band. (b) The upper band. [Color figure can be viewed in the online issue, which is available at www.interscience.wiley.com]

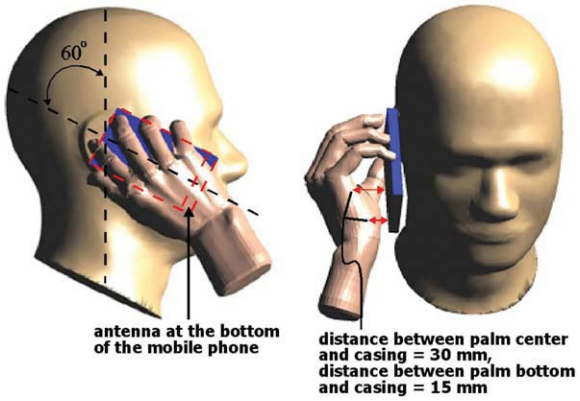

Frequency (MHz)		740	859	925	1795	1920	2045	2350	2595
1-g SAR (W/kg)	head only	0.84	0.99	1.14	0.62	0.61	0.53	0.26	0.20
	head and hand	0.84	0.96	1.18	0.81	1.15	1.30	0.71	1.86
Return loss (dB)	head only	8.3	7.1	8.6	9.4	11.8	10.4	6.4	7.7
	head and hand	11.7	7.9	9.5	7.7	9.1	7.7	4.6	9.1

Figure 10 SAR simulation model and the simulated SAR values for 1-g tissue for the proposed antenna. The return loss given in the table shows the impedance matching level at the testing frequency. [Color figure can be viewed in the online issue, which is available at www.interscience.wiley.com]

phantom. Except at 2595 MHz for 1-g head and hand tissue, the obtained SAR values for the proposed antenna are below the SAR limit of 1.6 W/kg [19]. For practical applications with electronic components loaded on the system circuit board, some of which are usually lossy elements, the obtained SAR values for the antenna over all the eight operating bands with the presence of the user's head and hand are still very promising to meet the required SAR limit of 1.6 W/kg.

4. CONCLUSIONS

An eight-band LTE/WWAN mobile phone antenna with a small size formed by a simple two-strip structure excited by an internal distributed LC matching circuit has been proposed, fabricated, and tested. The proposed antenna can be mounted at the small no-ground portion of 10×60 mm^2 on the system circuit board of the mobile phone and shows a thin thickness of 3 mm only. With proper selection of the dimensions of the distributed LC matching circuit, which comprises the coupling feed as a capacitive element and the shorting strip as an inductive element, leads to the excitation of two wide operating bands for the simple two-strip antenna to cover the desired 698–960 and 1710–2690 MHz bands. Good radiation characteristics for frequencies over the eight operating bands have been obtained. The obtained SAR values for the proposed antenna are also promising to meet the SAR limit for practical mobile phone applications.

REFERENCES

1. K.L. Wong and C.H. Huang, Bandwidth-enhanced internal PIFA with a coupling feed for quad-band operation in the mobile phone, Microwave Opt Technol Lett 50 (2008), 683–687.
2. K.L. Wong and C.H. Huang, Printed PIFA with a coplanar coupling feed for penta-band operation in the mobile phone, Microwave Opt Technol Lett 50 (2008), 3181–3186.
3. C.H. Chang and K.L. Wong, Internal coupled-fed shorted monopole antenna for GSM850/900/1800/1900/UMTS operation in the laptop computer, IEEE Trans Antennas Propag 56 (2008), 3600–3604.
4. K.L. Wong and S.J. Liao, Uniplanar coupled-fed printed PIFA for WWAN operation in the laptop computer, Microwave Opt Technol Lett 51 (2009), 549–554.
5. K.L. Wong and C.H. Huang, Compact multiband PIFA with a coupling feed for internal mobile phone antenna, Microwave Opt Technol Lett 50 (2008), 2487–2491.
6. C.T. Lee and K.L. Wong, Uniplanar coupled-fed printed PIFA for WWAN/WLAN operation in the mobile phone, Microwave Opt Technol Lett 51 (2009), 1250–1257.
7. C.H. Chang and K.L. Wong, GSM850/900/1800/1900/UMTS coupled-fed planar λ/8-PIFA for internal mobile phone antenna, Microwave Opt Technol Lett 51 (2009), 1091–1096.
8. C.H. Chang and K.L. Wong, Printed λ/8-PIFA for penta-band WWAN operation in the mobile phone, IEEE Trans Antennas Propag 57 (2009), 1373–1381.
9. W.Y. Chen and K.L. Wong, Small-size coupled-fed shorted T-monopole for internal WWAN antenna in the slim mobile phone, Microwave Opt Technol Lett 52 (2010), 257–262.
10. C.H. Chang and K.L. Wong, Small-size printed monopole with a printed distributed inductor for penta-band WWAN mobile phone application, Microwave Opt Technol Lett 51 (2009), 2903–2908.
11. Y.W. Chi and K.L. Wong, Quarter-wavelength printed loop antenna with an internal printed matching circuit for GSM/DCS/PCS/UMTS operation in the mobile phone, IEEE Trans Antennas Propag 57 (2009), 2541–2547.
12. K.L. Wong and T.W. Kang, GSM850/900/1800/1900/UMTS printed monopole antenna for mobile phone application, Microwave Opt Technol Lett 50 (2008), 3192–3198.
13. T. Oshiyama, Multi-band antenna, U.S. Patent Application Publication No. US 2007/0249313 A1, Oct. 25, 2007.
14. M. Tzortzakakis and R.J. Langley, Quad-band internal mobile phone antenna, IEEE Trans Antennas Propag 55 (2007), 2097–2103.
15. Z. Zhang, J.-C. Langer, K. Li, and M.F. Iskander, Design of ultra-wideband mobile phone stubby antenna (824 MHz–6 GHz), IEEE Trans Antennas Propag 56 (2008), 2107–2111.
16. S. Sesia, I. Toufik, and M. Baker (Eds.), LTE, the UMTS long term evolution: From theory to practice, Wiley, New York, 2009.
17. G. Park, M. Kim, T. Yang, J. Byun, and A.S. Kim, The compact quad-band mobile handset antenna for the LTE700 MIMO application, In: Proceedings of the IEEE Antennas and Propagation Society International Symposium, Charleston, SC, 2009, Session 307.
18. K.L. Wong, Planar antennas for wireless communications, Wiley, New York, 2003.
19. American National Standards Institute (ANSI), Safety levels with respect to human exposure to radio-frequency electromagnetic field, 3 kHz to 300 GHz, ANSI/IEEE Standard C95.1, Boulder, CO, 1999.
20. C.H. Li, E. Ofli, N. Chavannes, and N. Kuster, Effects of hand phantom on mobile phone antenna performance, IEEE Trans Antennas Propag 57 (2009), 2763–2770.
21. H.C. Tung, T.F. Huang, and C.Y. Lin, Shorted monopole dual band antenna for ultra-thin profile slider mobile phone, In: Proceedings of the 2006 IEEE AP-S International Symposium Digest, Albuquerque, NM, pp. 4693–4696.
22. K.L. Wong, Y.C. Lin, and T.C. Tseng, Thin internal GSM/DCS patch antenna for a portable mobile terminal, IEEE Trans Antennas Propag 54 (2006), 238–242.
23. K.L. Wong, Y.C. Lin, and B. Chen, Internal patch antenna with a thin air-layer substrate for GSM/DCS operation in a PDA phone, IEEE Trans Antennas Propag 55 (2007), 1165–1172.
24. R.A. Bhatti, Y.T. Im, J.H. Choi, T.D. Manh, and S.O. Park, Ultra-thin planar inverted-F antenna for multistandard handsets, Microwave Opt Technol Lett 50 (2008), 2894–2897.
25. C.I. Lin and K.L. Wong, Printed monopole slot antenna for internal multiband mobile phone antenna, IEEE Trans Antennas Propag 55 (2007), 3690–3697.

26. H. Rhyu, J. Byun, F.J. Harakiewicz, M.J. Park, K. Jung, D. Kim, N. Kim, T. Kim, and B. Lee, Multi-band hybrid antenna for ultra-thin mobile phone applications, Electron Lett 45 (2009), 773–334.
27. Ansoft Corporation HFSS. Available at: http://www.ansoft.com/products/hf/hfss/.
28. SEMCAD, Schmid & Partner Engineering AG (SPEAG). Available at: http://www.semcad.com.
29. C.T. Lee and K.L. Wong, Internal WWAN clamshell mobile phone antenna using a current trap for reduced groundplane effects, IEEE Trans Antennas Propag 57 (2009), 3303–3308.

TEMPERATURE-INDEPENDENT FIBER BRAGG GRATING TILT SENSOR

Kai Ni,[1,2] Xinyong Dong,[2] Yongxing Jin,[2] and Haisong Xu[1]
[1] State Key Laboratory of Modern Optical Instrumentation, Zhejiang University, Hangzhou, Zhejiang 310027, China; Corresponding author: zjnk2004@hotmail.com
[2] Institute of Optoelectronic Technology, China Jiliang University, Hangzhou, Zhejiang 310018, China

Received 4 January 2010

ABSTRACT: *A novel fiber Bragg grating (FBG) tilt sensor is proposed to detect the magnitude and the direction of a two-dimensional inclination by using four FBGs. High angle sensitivity and measurement resolution have been achieved, and the temperature effect has been eliminated completely without additional temperature compensation schemes. Experimental results verified the feasibility of the proposed idea.* © 2010 Wiley Periodicals, Inc. Microwave Opt Technol Lett 52:2250–2252, 2010; Published online in Wiley InterScience (www.interscience.wiley.com). DOI 10.1002/mop.25425

Key words: *fiber Bragg gratings (FBGs); fiber-optic sensors; temperature-insensitive; tilt measurement*

1. INTRODUCTION

Fiber Bragg gratings (FBGs) have been widely used as sensors for the measurement of temperature, strain [1–3], pressure [4], force [5], acceleration [6], and tilt angle [7–9]. The basic principle of FBG sensors is based on the modulation of the reflection wavelength of FBGs in response to the measurands, such as temperature and strain. Tilt sensors (also known as inclinometers) are required for measuring the angular deflection of an object against a reference plane or line. They are frequently used in the field of aviation (e.g., monitoring for aircraft landing) and civil engineering (e.g., monitoring the inclination of towers and bridge holders). They can also apply to platform levering, boom angle indication, slope angle measurement, etc. Most conventional tilt sensors are realized by transforming the inclination into electric signals through a magnetic effect [10, 11] or capacitive effect [12]. Optical interferometry was also applied to the tilt angle measurement with about the same resolution [13]. Compared with other types of sensors, FBG sensors have advantages of being inherently self-referencing and the capability in multiplexing. A FBG-based tilt sensor was reported in [7], where a pendulum scheme with two pairs of FBGs was used. The wavelength separation between the FBGs in each pair is used as the encoding signal so that the temperature effect was eliminated. The sensor configuration, however, was complex so that errors may be introduced by the structure instability or nonideal force transfer from the pendulum to the FBGs. In this article, we report a new FBG tilt sensor based on four FBGs, which possesses a more simple and stable configuration and hence a relatively high measurement accuracy. Preliminary results were achieved which verified the feasibility of the proposed tilt sensor design. High tilt angle measurement accuracy and resolution were demonstrated.

2. PRINCIPLE

The tilt sensor consists of a weight hanged to a circular plate through four equal-long optical fibers on which FBGs were inscripted in-between, as shown in Figure 1. Bonding points of the four fibers on the brim of the circular plate were separated equally so that each pair of FBGs with the opposite position can sense the inclination in the plane they belong without cross sensitivity.

The position of the weight was kept in equilibrium by the four optical fibers, so all the four fibers were prestrained equally. The initial strain and reflection wavelengths of the FBGs are denoted by ε_0 and $\lambda_{i\,=\,1,2,3,4}$, respectively. When tilt is applied to the sensor from the initial position, where the force and strains of the four fibers are the same, the force and strain induced in the fibers will be changed. If we consider an inclination of α occurred in the x-y plane and an inclination β occurred in the y-z plane, the equilibrium equation for the weight is given by

$$SE(\varepsilon_0 + \Delta\varepsilon_3)\frac{r}{l} - SE(\varepsilon_0 + \Delta\varepsilon_1)\frac{r}{l} - mg\sin\alpha = 0 \tag{1}$$

and

$$SE(\varepsilon_0 + \Delta\varepsilon_4)\frac{r}{l} - SE(\varepsilon_0 + \Delta\varepsilon_2)\frac{r}{l} - mg\sin\beta = 0 \tag{2}$$

where S is the area of the cross section of the fiber, E is the Young's modulus of the host material of the fiber, m is the mass of the weight, g is the gravitational acceleration, and r and l are the length of radius of the circular plate and the distance from weight to the brim of the circular plate, respectively. Equations (1) and (2) can be simplified as

$$\Delta\varepsilon_3 - \Delta\varepsilon_1 = \frac{mgl}{SEr}\sin\alpha \tag{3}$$

and

$$\Delta\varepsilon_4 - \Delta\varepsilon_2 = \frac{mgl}{SEr}\sin\beta. \tag{4}$$

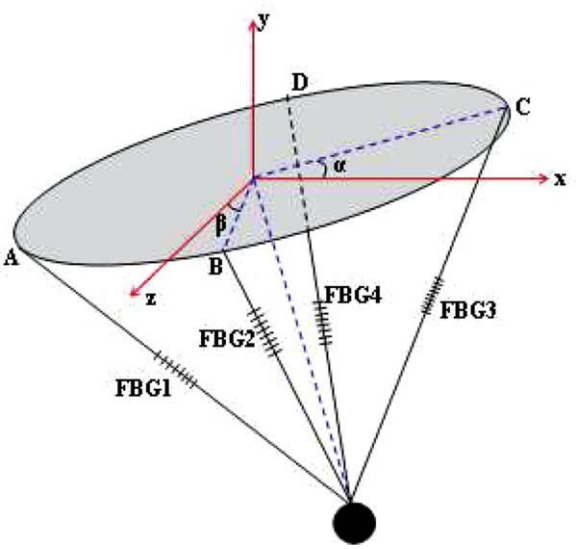

Figure 1 Schematic diagram of the proposed FBG tilt sensor. [Color figure can be viewed in the online issue, which is available at www.interscience.wiley.com]